A Modified Mode-Matching Technique and Its Application to a Class of Quasi-Planar Transmission Lines

RUEDIGER VAHLDIECK, MEMBER IEEE, AND JENS BORNEMANN

Abstract — **A rigorous and versatile hybrid-mode analysis is presented to determine the normalized propagation constants in a class of quasi-planar transmission-line structures.**

The method is accurate and covers the finite metallization thickness, mounting grooves, and an arbitrary number of dielectric subregions.

Utilizing a modified mode-matching technique, one can derive discontinuity and transmission-line matrices for each homogeneous subregion. Successively multiplying matrix equations of all subregions leads to the characteristic matrix system. This procedure makes it possible to create a modularized computer program which can be conveniently extended to a wide spectrum of conceivable configurations simply by inserting the matrix equations of additional subregions in the multiplication process. To demonstrate the efficiency of the proposed method, dispersion characteristics of dominant and next higher order hybrid modes in earthed and insulated finlines, suspended microstrips, and coupled striplines with tuning septa, are given as examples.

I. INTRODUCTION

E-PLANE MILLIMETER-WAVE integrated circuits are of considerable interest in systems requiring single-mode broad-band operation. Earthed and insulated finlines, coupled strip- and coplanar lines are the most common structures which have been succesfully applied, for example, in the design of broad-band directional couplers, taper sections, and filters. Their propagation characteristics have been obtained by various methods. An early paper by Meier [1] describes the dominant mode in an earthed finline as a variation of the corresponding mode in a ridged waveguide, but test measurements are still necessary to determine the equivalent dielectric constant of the configuration. In order to avoid these time-consuming and expensive measurements, several theoretical methods have been proposed to evaluate the dispersion characteristics of the dominant and sometimes even higher order modes in an earthed finline or more complicated configurations like coupled strip or coplanar lines.

The two-dimensional transmission-line matrix (TLM) has been applied by Shih and Hoefer [2] to determine the dominant and second-order mode cutoff frequencies in a unilateral, bilateral, and so-called insulated finline. More complicated structures have been analyzed by using the numerically very efficient spectral-domain method (SDM) (Itoh and Schmidt [3]–[5]), but only results with zero metallization thickness and neglected mounting grooves have been published.

More recently, two different mathematical treatments have been presented which take into account the finite metallization thickness (Kitazawa and Mittra [13]) and, additionally, the mounting grooves (Vahldieck [6] and Bornemann [7]). In [13], a hybrid-mode formulation has been proposed in which Green's functions are derived using conventional circuit theory. Results are given for unilateral and bilateral finlines.

Vahldieck [6] and Bornemann [7] extended a modified mode-matching technique which utilizes a transverse resonance relation [8], [14] to reduce the number of required eigenvalue equations. This method, which includes both the finite metallization thickness and the mounting grooves, has been applied successfully to a generalized finline configuration with more than one dielectric subregion and different fin thicknesses [6]. In [7], structures containing both a strip and a slot were treated, and results were presented for coupled slotlines and suspended microstrips. This already indicates that the method is quite general and can be extended very easily to more complicated combinations of strip- and slotlines.

For the numerical computation of the propagation constants, it is an advantage of this method that the order of the characteristic matrix equation is only $2NH-1$ (where NH is the number of orthogonal eigenfunctions considered in each subregion) and remains constant even for an increasing number of transverse discontinuities. This is in contrast, for example, to the well-known mode-matching procedure used by Siegl [11] and Beyer [12] in which the size of the characteristic matrix equation usually increases with the number of subregions. Moreover, in the latter method, all boundary conditions are satisfied before the tangential E- and H-fields at each interface are matched. This leads to an inflexible procedure and makes it normally necessary to create a new computer program when investigating different configurations with additional subregions.

However, the modified mode-matching technique combined with a transverse resonance relation avoids this disadvantage. Initially, the boundary conditions at the waveguide sidewalls ($x=0$ and $x=a$, Fig. 1(a)–(c)) are neglected. The configuration can then be regarded as a

Manuscript received February 5, 1985; revised May 31, 1985.

R. Vahldieck is with the Department of Electrical Engineering, University of Ottawa, 770 King Edward Ave., Ottawa, Ontario K1N 6N5, Canada.

J. Bornemann is with the Microwave Department, University of Bremen, D-2800 Bremen 33, Kufsteiner Str., NW1, West Germany.

0018-9480/85/1000-0916$01.00

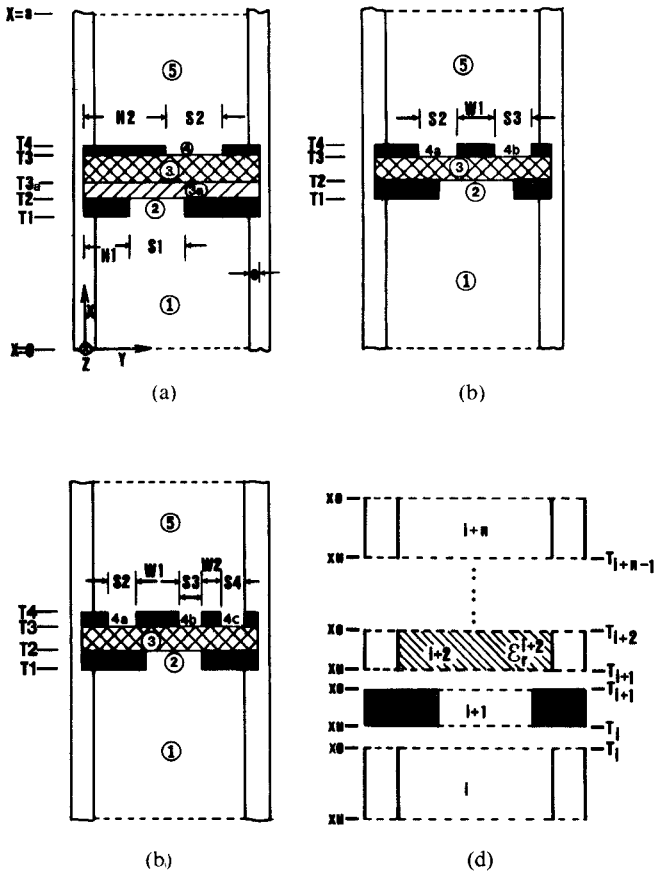

Fig. 1. Some general cross sections of quasi-planar transmission lines. (a) Earthed bilateral finline, (b) coupled slotline, (c) coupled suspended stripline, (d) subdivision of a cross section into an arbitrary number of homogeneous subregions.

parallel-plate line subdivided into homogeneous cross sections (Fig. 1(d)) in which partial wave amplitudes are defined, traveling in positive and negative x-directions with the still unknown propagation constant kx. After the elimination of the field coefficients in each subregion, a transverse transmission-line matrix results which relates the amplitudes at the lower ($x = xu$) and the upper boundary ($x = xo$, cf., Fig. 1(d)) of a subregion. Satisfying a modified field-matching condition at the common interfaces (e.g., T_l, Fig. 1(d)) transforms the partial wave amplitudes of cross-section i into those of cross-section $i+1$. Successively multiplying each transformation matrix with the appropriate transmission-line matrix of the corresponding subregion, a relation only between the partial wave amplitudes at the lower ($x = 0$) and upper ($x = a$) boundary of the waveguide is obtained. Finally, the inhomogeneous waveguide cross section can be regarded as a line resonator in which the resonance condition is satisfied by inserting the up-to-now neglected boundary conditions at the metallic sidewalls ($x = 0$ and $x = a$). This procedure reduces the size of the characteristic matrix equation to a quarter of the original size. Furthermore, it makes the method very flexible because an arbitrary number of subregions can be inserted easily in the matrix system simply by multiplying the additional transformation and transmission-line matrices with the previous.

The aim of this paper is to demonstrate the potential of this versatile and accurate treatment. As examples, earthed and insulated finlines will be analyzed, as well as coupled strip- and coupled slotlines. Finally, some detailed results on the effect of finite metallization thickness and mounting grooves on the dispersion characteristics of quasi-TEM, and next higher order hybrid modes will be presented.

II. Theory

Since the theoretical treatment has been described recently by Vahldieck [6] and Bornemann [7], only the principle steps will be explained. For further information, the reader is referred to [6] and [7].

It is well known that quasi-planar transmission lines support hybrid modes in which all six field components can occur. The transversely inhomogeneous configuration is divided into homogeneous subregions. In each of these subregions, the hybrid fields

$$\vec{E}^i = \nabla \times \nabla \times \vec{A}_e^i - j\omega\mu \nabla \times \vec{A}_m^i \tag{1}$$

$$\vec{H}^i = \nabla \times \nabla \times \vec{A}_m^i + j\omega\epsilon^i \nabla \times \vec{A}_e^i \tag{2}$$

can be expressed by a superposition of the axial z-components of two independent Hertzian vector potentials $\vec{A}_m$ and $\vec{A}_e$. The potential functions are a sum of suitable orthogonal eigenfunctions

$$\left.\begin{aligned} A_{mz}^i &= \sum_n^\infty f_{c(n)}^i(y) \cdot I_{m(n)}^i(x) \\ A_{ez}^i &= \sum_n^\infty f_{s(n)}^i(y) \cdot U_{e(n)}^i(x) \end{aligned}\right\} \cdot e^{-jkz \cdot z} \tag{3, 4}$$

which satisfy the boundary condition at the metallic surface and obeys the scalar Helmholtz equation. Initially, however, we neglect the boundary conditions at the waveguide sidewalls ($x = 0$ and $x = a$, cf., Fig. 1) and regard each subregion as a part of a parallel-plate line in which partial wave amplitudes I_m^i and U_e^i are defined and travel in positive and negative x-directions. This procedure results in a somewhat higher theoretical effort, but is necessary in order to reduce the size of the characteristic matrix equation. Finally, it makes it easy to implement any desired number of subregions in the formulation. The functions f_c and f_s in (3) and (4) (given in the Appendix) implicitly satisfy the y-dependent boundary conditions in their respective subregions. I_m^i and U_e^i, as well as their derivatives

$$U_m^i = \frac{dI_m^i}{dx} \quad \text{and} \quad I_e^i = \frac{dU_e^i}{dx}$$

combined as vectors $\boldsymbol{U}^i$ and $\boldsymbol{I}^i$ at the upper boundary ($x = xo$) of each subregion, can be determined from the amplitudes at the lower boundary ($x = xu$), see Fig. 1(d). Therefore, a generalized transmission-line matrix $\boldsymbol{R}^i$ can be found which relates $\boldsymbol{U}^i$ and $\boldsymbol{I}^i$ at the two coordinates as follows:

$$\begin{bmatrix} \boldsymbol{U}^i \\ \boldsymbol{I}^i \end{bmatrix}_{x=xo} = \underbrace{\begin{bmatrix} \boldsymbol{R}_c^i & \boldsymbol{R}_s^i \\ \boldsymbol{R}_s^{i'} & \boldsymbol{R}_c^i \end{bmatrix}}_{\boldsymbol{R}^i} \cdot \begin{bmatrix} \boldsymbol{U}^i \\ \boldsymbol{I}^i \end{bmatrix}_{x=xo} \tag{5}$$

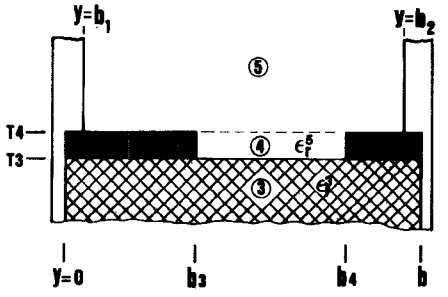

(a)

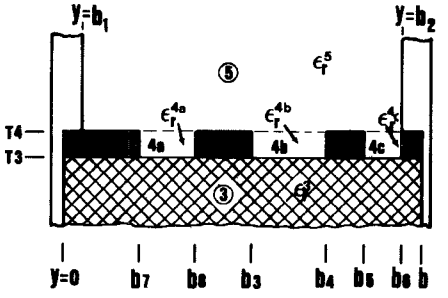

(b)

Fig. 2. Representative transition T4 and T3 for the configurations in Fig. 1. (a) Slot transition with only one slot. (b) Slot transition with three slots.

$\boldsymbol{R}_c^i$, $\boldsymbol{R}_s^i$, and $\boldsymbol{R}_c^i$, are diagonal matrices containing sine and cosine functions. They are explained in the Appendix. Before a final relation between the amplitude vectors at the upper ($x = a$) and the lower ($x = 0$) sidewall of the waveguide can be given, it is necessary to modify the continuity equations at each transverse discontinuity, such that the amplitude vectors of subregion $i+1$, for example, are determined by those of region i.

The following mathematical derivation of this principle step is based on the representative transition $T4$ in Fig. 2. In the first case of Fig. 2(a), the continuity condition can be written as follows:

$$E_{y,z}^5 = E_{y,z}^4 \tag{6}$$

$$E_{y,z}^5 = 0, \qquad b_1 \leqslant y < b_3, \quad b_4 < y \leqslant b_2 \tag{6a}$$

$$H_{y,z}^5 = H_{y,z}^4, \qquad b_3 \leqslant y \leqslant b_4 \tag{7}$$

and in the second case of Fig. 2(b) in plane $T4$

$$E_{y,z}^5 = \sum_\nu E_{y,z}^\nu \tag{8}$$

$$E_{y,z}^5 = 0, \qquad b_1 \leqslant y < b_7, b_8 < y < b_3, b_4 < y < b_5 \tag{8a}$$

$$H_{y,z}^5 = H_{y,z}^\nu, \qquad b_7 \leqslant y \leqslant b_8, b_3 \leqslant y \leqslant b_4, b_5 \leqslant y \leqslant b_2 \quad (\nu \in 4a, 4b, 4c). \tag{9}$$

In order to determine the partial wave amplitudes of subregion $i = 5$ (Fig. 2(a)) from their corresponding amplitudes in the adjacent area $i = 4$, we first modify (6) and (7) such that the following expressions result:

$$E_y: \frac{\partial A_{mz}^5}{\partial x} = \frac{\partial A_{mz}^4}{\partial x} - K_\mu^4(\omega, kz)\frac{\partial A_{ez}^4}{\partial y} \tag{10}$$

$$E_z: \quad A_{ez}^5 = K^4(\omega, kz) A_{ez}^4 \tag{11}$$

$$H_z: \quad A_{mz}^5 = K^4(\omega, kz) A_{mz}^4 \tag{12}$$

$$H_y: \frac{\partial A_{ez}^5}{\partial x} = \frac{\epsilon_r^4}{\epsilon_r^5}\frac{\partial A_{ez}^4}{\partial x} + K_\epsilon^4(\omega, kz)\frac{\partial A_{mz}^4}{\partial y} \tag{13}$$

with

$$K^4(\omega, kz) = \frac{\epsilon_r^4 - \beta^2}{\epsilon_r^5 - \beta^2}, \qquad \beta = kz/ko$$

$$K_\mu^4(\omega, kz) = \frac{kz}{\omega\mu}(1 - K^4(\omega, kz))$$

$$K_\epsilon^4(\omega, kz) = \frac{kz}{\omega\epsilon^5}(1 - K^4(\omega, kz))$$

and similarly for (8) and (9)

$$E_y: \qquad \frac{\partial A_{mz}^5}{\partial x} = \sum_\nu \left[\frac{\partial A_{mz}^\nu}{\partial x} - K_\mu^\nu(\omega, kz)\frac{\partial A_{ez}^\nu}{\partial y}\right] \tag{14}$$

$$Ez: \qquad A_{ez}^5 = \sum_\nu K^\nu(\omega, kz) A_{ez}^\nu \tag{15}$$

$$Hz: \bar{K}^\nu(\omega, kz) A_{mz}^5 = A_{mz}^\nu \tag{16}$$

$$H_y: \frac{\epsilon_r^5}{\epsilon_r^\nu}\frac{\partial A_{ez}^5}{\partial x} + \bar{K}_\epsilon^\nu(\omega, kz)\frac{\partial A_{mz}^5}{\partial y} = \frac{\partial A_{ez}^\nu}{\partial x} \tag{17}$$

with

$$\bar{K}_\epsilon^\nu(\omega, kz) = \frac{kz}{\omega\epsilon^\nu}(1 - \bar{K}^\nu(\omega, kz))$$

$$\bar{K}^\nu(\omega, kz) = \frac{\epsilon_r^5 - \beta^2}{\epsilon_r^\nu - \beta^2}$$

$$K_\mu^\nu(\omega, kz) = \frac{kz}{\omega\mu}(1 - K^\nu(\omega, kz)).$$

For the interface $T3$ (Fig. 2(a)), replace in (10)–(13) the index $i = 5$ with $i = 4$, and index $i = 4$ with $i = 3$. To obtain the interface expression for $T3$ in Fig. 2(b), replace in (14)–(17) $i = 5$ with $i = 3$. The discontinuities $T4$, $T3$ in Fig. 1(b) are then also included in (14)–(17). Moreover, the equation system (10)–(17) is very instructive. It shows that the coupling between TE and TM waves is automatically included, and that only in structures with homogeneously filled cross sections (e.g., ridged waveguide) or in inhomogeneously filled structures at cutoff ($kz = 0$) are these wave types decoupled since $K\mu\ (\omega, kz)$ and $K\epsilon\ (\omega, kz)$ in (10) and (13) vanish as well as $K\mu\ (\omega, kz)$ and $K\epsilon\ (\omega, kz)$ in (14) and (17).

Multiplication of the above equation system with appropriate orthogonal eigenfunctions [6], [7] separates the

partial wave amplitudes on the left-hand side of (10)–(13)

$$\underset{x=T_4}{\begin{bmatrix} \boldsymbol{um}^5 \\ \boldsymbol{Ue}^5 \end{bmatrix}} = \underbrace{\begin{bmatrix} \frac{2}{b_2-b_1}\boldsymbol{Fc}^4 & K_\mu^4(\omega,kz)\widetilde{\boldsymbol{Fc}}^4 \\ \mathbf{0} & \frac{2}{b_2-b_1}K^4(\omega,kz)\boldsymbol{Fs}^4 \end{bmatrix}}_{\boldsymbol{V}^E} \cdot \underset{x=T_4}{\begin{bmatrix} \boldsymbol{Um}^4 \\ \boldsymbol{Ue}^4 \end{bmatrix}} \tag{18}$$

$$\underset{x=T_4}{\begin{bmatrix} \boldsymbol{Im}^5 \\ \boldsymbol{Ie}^5 \end{bmatrix}} = \underbrace{\begin{bmatrix} \frac{b_4-b_3}{2}K^4(\omega,kz)(\boldsymbol{Fc}^{4T})^{-1} & \mathbf{0} \\ -K_\epsilon^4(\omega,kz)(\widetilde{\boldsymbol{Fs}}^{4T})^{-1} & \frac{b_4-b_3}{2}\frac{\epsilon_r^4}{\epsilon_r^5}(\boldsymbol{Fs}^{4T})^{-1} \end{bmatrix}}_{\boldsymbol{V}^H} \cdot \underset{x=T_4}{\begin{bmatrix} \boldsymbol{Im}^4 \\ \boldsymbol{Ie}^4 \end{bmatrix}} \tag{19}$$

and similary in (14)–(17)

$$\underset{x=T_4}{\begin{bmatrix} \boldsymbol{Um}^5 \\ \boldsymbol{Ue}^5 \end{bmatrix}} = \underbrace{\begin{bmatrix} \frac{2}{b_2-b_1}\boldsymbol{Fc}^{4^a} & \frac{2}{b_2-b_1}\boldsymbol{Fc}^{4^b} & \frac{2}{b_2-b_1}\boldsymbol{Fc}^{4^c} & -K_\mu^{4^a}(\omega,kz)\widetilde{\boldsymbol{Fc}}^{4^a} & -K_\mu^{4^b}(\omega,kz)\widetilde{\boldsymbol{Fc}}^{4^b} & -K_\mu^{4^c}(\omega,kz)\widetilde{\boldsymbol{Fc}}^{4^c} \\ \mathbf{0} & \mathbf{0} & \mathbf{0} & \frac{2}{b_2-b_1}K^{4^a}(\omega,kz)\boldsymbol{Fs}^{4^a} & \frac{2}{b_2-b_1}K^{4^b}(\omega,kz)\boldsymbol{Fs}^{4^b} & \frac{2}{b_2-b_1}K^{4^c}(\omega,kz)\boldsymbol{Fs}^{4^c} \end{bmatrix}}_{\boldsymbol{Vs}^E} \cdot \underset{x=T_4}{\begin{bmatrix} \boldsymbol{Um}^{4^a} \\ \boldsymbol{Um}^{4^b} \\ \boldsymbol{Um}^{4^c} \\ \boldsymbol{Ue}^{4^a} \\ \boldsymbol{Ue}^{4^b} \\ \boldsymbol{Ue}^{4^c} \end{bmatrix}} \tag{20}$$

$$\underbrace{\begin{bmatrix} \bar{K}^{4^a}(\omega,kz)\dfrac{2}{b_8-b_7}\boldsymbol{Fc}^{4^{aT}} & \mathbf{0} \\ \bar{K}^{4^b}(\omega,kz)\dfrac{2}{b_4-b_3}\boldsymbol{Fc}^{4^{bT}} & \mathbf{0} \\ \bar{K}^{4^c}(\omega,kz)\dfrac{2}{b_6-b_5}\boldsymbol{Fc}^{4^{cT}} & \mathbf{0} \\ \bar{K}_\epsilon^{4^a}(\omega,kz)\dfrac{2}{b_8-b_7}\widetilde{\boldsymbol{Fs}}^{4^{aT}} & \dfrac{\epsilon_{r^5}}{\epsilon_{r^{4a}}}\dfrac{2}{b_8-b_7}\boldsymbol{Fs}^{4^{aT}} \\ \bar{K}_\epsilon^{4^b}(\omega,kz)\dfrac{2}{b_4-b_3}\widetilde{\boldsymbol{Fs}}^{4^{bT}} & \dfrac{\epsilon_{r^5}}{\epsilon_{r^{4b}}}\dfrac{2}{b_4-b_3}\boldsymbol{Fs}^{4^{bT}} \\ \bar{K}_\epsilon^{4^c}(\omega,kz)\dfrac{2}{b_6-b_5}\widetilde{\boldsymbol{Fs}}^{4^{cT}} & \dfrac{\epsilon_{r^5}}{\epsilon_{r^{4c}}}\dfrac{2}{b_6-b_5}\boldsymbol{Fs}^{4^{cT}} \end{bmatrix}}_{\boldsymbol{Vs}^H}$$

$$\cdot \underset{x=T_4}{\begin{bmatrix} \boldsymbol{Im}^5 \\ \boldsymbol{Ie}^5 \end{bmatrix}} = \underset{x=T_4}{\begin{bmatrix} \boldsymbol{Im}^{4^a} \\ \boldsymbol{Im}^{4^b} \\ \boldsymbol{Im}^{4^c} \\ \boldsymbol{Ie}^{4^a} \\ \boldsymbol{Ie}^{4^b} \\ \boldsymbol{Ie}^{4^c} \end{bmatrix}}. \quad (21)$$

In the above equation system, $\boldsymbol{F}_c$ and $\boldsymbol{F}_s$ denote the coupling matrices. Combining vectors $\boldsymbol{U}_e$ and $\boldsymbol{U}_m$ into $\boldsymbol{U}$ as well as $\boldsymbol{I}_m$ and $\boldsymbol{I}_e$ into $\boldsymbol{I}$ finally yields the transformation matrix for the discontinuity $T4$ in Fig. 2(a)

$$\underset{x=T_4}{\begin{bmatrix} \boldsymbol{U}^5 \\ \boldsymbol{I}^5 \end{bmatrix}} = \underbrace{\begin{bmatrix} \boldsymbol{V}^E & \mathbf{0} \\ \mathbf{0} & \boldsymbol{V}^H \end{bmatrix}}_{\boldsymbol{V}^4} \cdot \underset{x=T_4}{\begin{bmatrix} \boldsymbol{U}^4 \\ \boldsymbol{I}^4 \end{bmatrix}} \quad (22)$$

or more generally

$$\underset{x=T_i}{\begin{bmatrix} \boldsymbol{U}^{i+1} \\ \boldsymbol{I}^{i+1} \end{bmatrix}} = \underbrace{\begin{bmatrix} \boldsymbol{V}^E & \mathbf{0} \\ \mathbf{0} & \boldsymbol{V}^H \end{bmatrix}}_{\boldsymbol{V}^i} \cdot \underset{x=T_i}{\begin{bmatrix} \boldsymbol{U}^i \\ \boldsymbol{I}^i \end{bmatrix}}.$$

Isolating the left-hand side amplitude vector $\boldsymbol{I}^5$ in (21) by multiplying with the inverse of matrix $\boldsymbol{Vs}^H$ yields a similar transformation matrix at the interface T^4 in Fig. 2(b).

$$\underset{x=T_4}{\begin{bmatrix} \boldsymbol{U}^5 \\ \boldsymbol{I}^5 \end{bmatrix}} = \underbrace{\begin{bmatrix} \boldsymbol{Vs}^E & \mathbf{0} \\ \mathbf{0} & (\boldsymbol{Vs}^H)^{-1} \end{bmatrix}}_{\boldsymbol{Vs}^4} \cdot \underset{x=T_4}{\begin{bmatrix} \boldsymbol{U}^{4^{a,b,c}} \\ \boldsymbol{I}^{4^{a,b,c}} \end{bmatrix}}. \quad (23)$$

Now, by successively multiplying the transmission-line matrix (5) of each subregion with the corresponding transformation matrix finally leads to the desired relation between amplitude vectors at the upper and lower waveguide sidewalls in the example of Fig. 1(c)

$$\underset{x=a}{\begin{bmatrix} \boldsymbol{U}^5 \\ \boldsymbol{I}^5 \end{bmatrix}} = \underbrace{\left[\boldsymbol{R}^5 \cdot \boldsymbol{Vs}^4 \cdot \boldsymbol{R}^{4^{a,b,c}} \cdot \boldsymbol{Vs}^3 \cdot \boldsymbol{R}^3 \cdot \boldsymbol{V}^2 \cdot \boldsymbol{R}^2 \cdot \boldsymbol{V}^1 \cdot \boldsymbol{R}^1\right]}_{\boldsymbol{G}} \cdot \underset{x=0}{\begin{bmatrix} \boldsymbol{U}^1 \\ \boldsymbol{I}^1 \end{bmatrix}}. \quad (24)$$

Inserting $\boldsymbol{V}^4 \cdot \boldsymbol{R}^4 \cdot \boldsymbol{V}^3$ instead of $\boldsymbol{Vs}^4 \cdot \boldsymbol{R}^v \cdot \boldsymbol{Vs}^3$ in (24) yields the matrix equation for the structure in Fig. 1(a), and (24) then reads as follows:

$$\underset{x=a}{\begin{bmatrix} \boldsymbol{U}^5 \\ \boldsymbol{I}^5 \end{bmatrix}} = \underbrace{\boldsymbol{R}^5 \prod_{i=1}^{5} \boldsymbol{V}^i \cdot \boldsymbol{R}^i}_{\boldsymbol{G}} \underset{x=0}{\begin{bmatrix} \boldsymbol{U}^1 \\ \boldsymbol{I}^1 \end{bmatrix}}. \quad (25)$$

The partial wave amplitudes are directly proportional to the field components $E_{y,z} \sim \boldsymbol{U}$ and $H_{z,y} \sim \boldsymbol{I}$, respectively. Hence, it follows for the up-to-now neglected boundary conditions (the transverse resonance condition) at the waveguide sidewalls, that $\boldsymbol{U} = \mathbf{0}$ (for $x = a$ and $x = 0$). Thus, the characteristic matrix equation is the upper-right quarter of the matrix product in both (25) and (24).

If NH is the number of summation terms in (3) and (4), $\boldsymbol{G}_{12}$ is of order $2NH-1$ and remains constant even for an increasing number of discontinuities. The zeros of its determinant provide the desired propagation constants

$$\det(\boldsymbol{G}_{12}(w,kz)) = 0. \quad (27)$$

It has thus been demonstrated that this method can handle generalized quasi-planar transmission-line configurations in which strips and slots are located arbitrarily in the waveguide; more than one dielectric subregion and different strip thicknesses in the same structure can be considered, as well as the finite depth of the mounting grooves.

In many practical cases, however, symmetry conditions can be included in the formulation process which make this general treatment as efficient as specialized procedures. If we consider, for example, a symmetrical bilateral finline with a symmetry plane at $x = T3$ (Fig. 1(a)), (25) can be written as follows:

$$\underset{x=T_3}{\begin{bmatrix} \boldsymbol{U}^3 \\ \boldsymbol{I}^3 \end{bmatrix}} = \boldsymbol{R}^3 \prod_{i=4}^{3} \boldsymbol{V}^i \cdot \boldsymbol{R}^i \underset{x=0}{\begin{bmatrix} \boldsymbol{U}^1 \\ \boldsymbol{I}^1 \end{bmatrix}}. \quad (28)$$

Thus, only three subregions ($i = 1,2,3$) have to be included in the entire multiplication procedure, which makes the numerical analysis more efficient. For a magnetic wall at $x = T3$, the new boundary condition can now be satisfied by setting $\boldsymbol{I}^3 = \mathbf{0}$, and the corresponding resonant condition changes the characteristic matrix equation from the upper-right quarter in (25) to the lower right in (28)

$$\mathbf{0} = \boldsymbol{G}_{22} \cdot \boldsymbol{I}^1. \quad (29)$$

For an electric wall at $x = T3$, however, the resonance condition is still the same as in the general case, and the characteristic matrix equation is again $\boldsymbol{G}_{12}$ in (28). Both submatrices ($\boldsymbol{G}_{22}$ and $\boldsymbol{G}_{12}$) can be solved independently and provide the propagation constants of all hybrid modes in symmetrical bilateral finlines. Other symmetry conditions may be implemented very easily so that solutions of a large spectrum of conceivable quasi-planar transmission-line configurations are available with only one general computer program.

For the numerical procedure, the infinite sum in (3) and (4) must be truncated after a certain number of terms. To

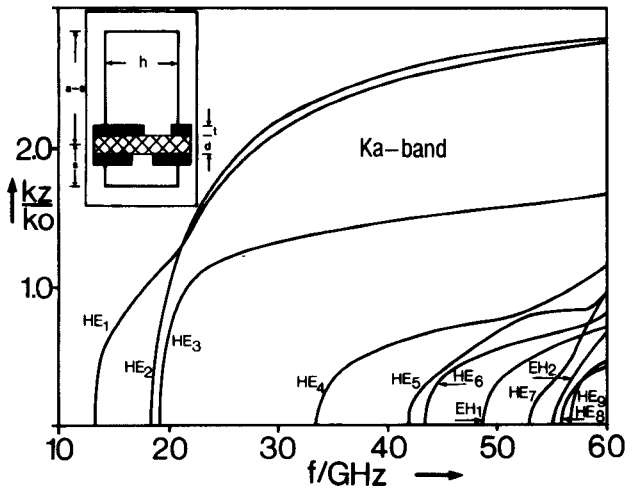

Fig. 3. Dispersion characteristic of an asymmetrical bilateral finline. $a = 7.112$ mm, $h = a/2$; $s = 2.2606$ mm, $H1 = 1.201$ mm, $s1 = 2.5$ mm, $H2 = 2.156$ mm, $s2 = 1.5$ mm, $e = 0.7$ mm; $d = 254.0$ μm, $\epsilon_r = 9.6$, $t = 70.0$ μm.

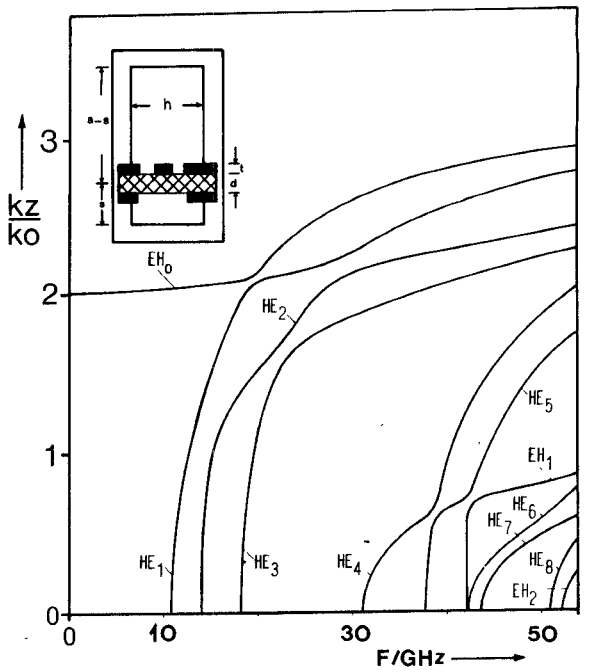

Fig. 4. Dispersion characteristic of a coupled slotline. $a = 7.112$ mm, $h = a/2$; $s = 1.778$ mm, $s1 = 2.2225$ mm, $H1 = 1.1557$ mm, $w1 = 0.592$ mm, $s2 = s3 = 0.592$ mm, $H2 = 1.3038$ mm; $d = 711.2$ μm, $\epsilon_r = 10.0$, $t = 71.0$ μm.

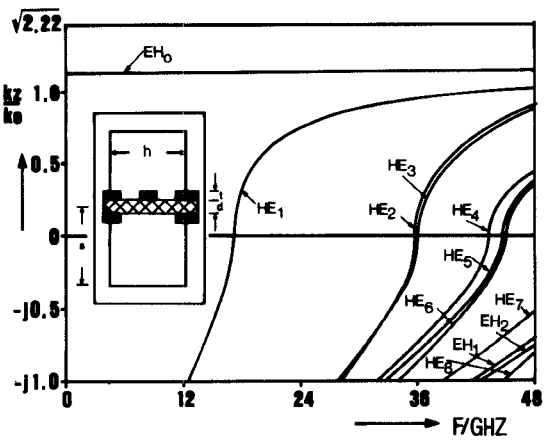

Fig. 5. Dispersion characteristic of a coupled slotline, centered in the waveguide. $a = 7.112$ mm, $h = a/2$; $s = 3.556$ mm, $s1 = 1.778$ mm, $w1 = 0.7112$ mm, $s2 = s3 = 0.7112$ mm; $d = 254.$ μm, $\epsilon_r = 2.22$, $t = 17.5$ μm.

achieve a 0.5-percent accuracy in the propagation constant and to overcome a relative convergence effect which usually occurs between 11–15 terms, a minimum of 17 and a maximum of 25 summation terms have been found to be sufficient for most configurations investigated. The amount of CPU time required to evaluate the propagation constant at one frequency sample is between 1–3 min on a VAX 11/750, but only a few seconds on a main-frame computer like a Siemens 7880. A higher accuracy is attainable by increasing the number of summation terms, but at the expense of increased CPU time.

The behavior of some dispersion curves presented below has been verified by increasing the truncation index NH to 30 to exclude numerical inaccuracies. Furthermore, all dispersion curves are labeled at cutoff. That implies that their notation beyond the cutoff frequencies remains the same even when some curves cross each other.

III. Results

First of all, the potential of the present method is demonstrated by calculating quasi-planar configurations arbitrarily located in the waveguide mount. Fig. 3 shows the dispersion behavior of a bilateral finline with a slot offset, asymmetric location, finite metallization thickness, and mounting grooves. All higher order hybrid modes are excited by an incident H_{10} wave, and it is a remarkable result that the HE_2 mode crosses the HE_1 mode resulting in a higher propagation constant than the intrinsic dominant mode for frequencies beyond 20 GHz. This is due to two causes. Firstly, both modes are strongly affected by the mounting grooves; secondly, the insert is stepped away from the center of the waveguide (towards the higher field concentration of the H_{20} mode of the empty waveguide).

In an asymmetrically suspended microstrip combined with a bilateral finline, this curious dispersion behavior is even more pronounced (Fig. 4). It is obvious that there exists an interaction between the hybrid eigenmodes resulting, for example, in nontypical dispersion curve of the EH_0 and HE_1 mode. However, this is no longer so when a still asymmetric transmission line is centered in the waveguide (Fig. 5).

Fig. 6 shows the dispersion of both quasi-TEM and first higher order hybrid modes in a shielded coupled stripline combined with a tuning septum. All strips and slots are arbitrarily located on the substrate. As shown in [3] and [5], the different phase velocities of both quasi-TEM modes can be equalized by tuning the slot on the opposite side of the strips (Fig. 7) which is a prior condition for the design of broad-band contradirectional couplers with high directivity. We have compared our results on the influence of slot width on the quasi-TEM-propagation constant with data given by Schmidt [5]. Agreement is very good, as

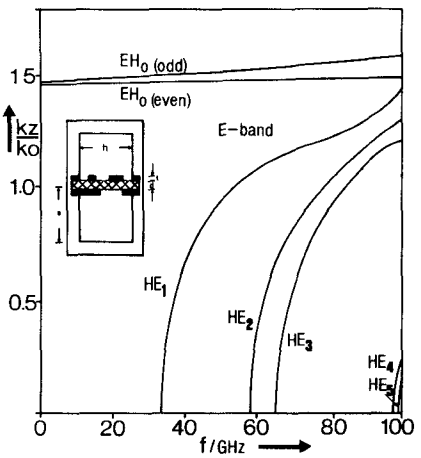

Fig. 6. Dispersion characteristic of a suspended coupled stripline centered in the waveguide but with arbitrarily located strips and slots. $a = 3.1$ mm, $h = a/2$; $s = a/2$, $s1 = 0.8$ mm, $s2 = 0.4$ mm, $s3 = 0.2$ mm, $s4 = 0.5$ mm, $w1 = 0.15$ mm, $w2 = 0.3$ mm, H1 = 1. mm, H2 = 0.5 mm; $d = 110.$ μm, $\epsilon_r = 3.75$, $t = 10.$ μm.

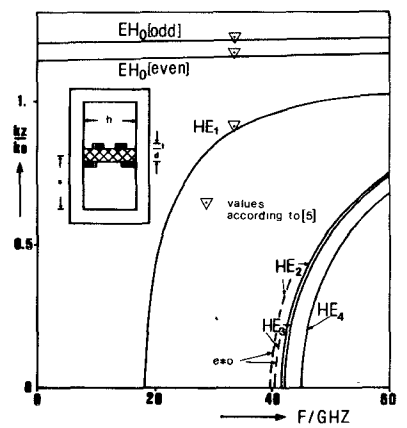

Fig. 7. Dispersion characteristic of a suspended coupled stripline compared with data given by [5]. $a = 7.112$ mm, $h = a/2$; $s = a/2$, $s1 = 0.2$ mm, $s2 = s4 = 1.378$ mm, $s3 = 0.4$ mm, $w1 = w2 = 0.2$ mm, $d = 254.$ μm, $\epsilon_r = 2.2$, $t = 5.$ μm; $e = 0$ (——), $e = 0.7$ mm (-----).

shown in Fig. 8. Moreover, Fig. 7 shows the dispersion characteristics of the configuration investigated in Fig. 8. Differences in the propagation constant are less than 2 percent. The optimal slot width which equalizes both quasi-TEM modes was measured in [9] and is given in Fig. 9. While theoretical values published in [10] show only a poor agreement with these experimental results, our data agree relatively well.

Considering a symmetry plane with an electric or magnetic wall at discontinuity, T3 in Fig. 1(a) yields a so-called insulated finline [2], [6] (both fins are connected with the waveguide mount). For the same symmetry plane in Fig. 1(b), a single-side insulated finline is obtained in which only one fin is not connected with the waveguide mount, and Fig. 1(c) provides a dual-side insulated finline. The last two types of transmission lines play an important role when active components are used and one or both fins have to be insulated by a gasket to allow a dc voltage to be developed across the fins. The bias is introduced at the mounting grooves. To simplify the numerical procedure for determining the fundamental mode in these structures, the depth of the grooves is assumed to be a quarter wavelength

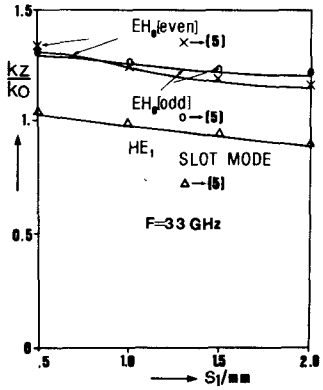

Fig. 8. Two coupled strips tuned by a slot on the opposite side of the dielectric. Dimensions identical to Fig. 7; $f = 33$ GHz; $e = 0$.

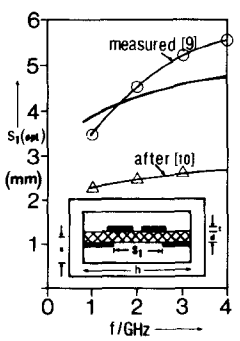

Fig. 9. Optimal slot width $S1$ (opt. in mm) of the tuning septum versus the frequency. $a = 7.27$ mm, $h = 25.$ mm; $s = a/2$, $w1 = w2 = 2.2$ mm, $s2 = s4 = 9.9$ mm, $s3 = 0.8$ mm; $d = 1.27$ mm, $\epsilon_r = 9.6$, $t = 17.5$ μm. measured [9], evaluated [10], —— this method.

at operating frequency and regarded as a choke section by which the RF continuity between the fins and the waveguide wall is achieved. Hence, the configuration has been investigated as an earthed finline. For practical application, however, these configurations support quasi-TEM modes, which can be seen in the following figures.

Fig. 10 presents the dispersion characteristics of a so-called insulated finline. A comparison with the configuration in Fig. 11, where only one fin is insulated, reveals the difference, which is essentially the occurence of the quasi-TEM mode (EH_0). In both cases, the HE_1 mode has almost the same cutoff frequency and is obviously not affected by the insulation of one fin. The insulation of both fins (Fig. 12) does not change the cutoff frequency of the HE_1 mode either, but a second quasi-TEM mode occurs as expected. Combining the single insulated with an earthed bilateral finline (Fig. 13) increases the propagation constant of EH_0 and decreases the cutoff frequencies of the higher order modes HE_2–HE_4. This tendency is also observed for the dual insulated finline in Fig. 14 and resembles somewhat the higher order mode behavior in an earthed bilateral finline [15]. Influences of the finite metallization thickness on the HE_1 and quasi-TEM modes are relatively small as can be seen from Fig. 15. A thicker metallization leads to decreasing quasi-TEM- and HE_1-mode propagation constants. This corresponds with the physical point of view that their electric fields are mainly concentrated in the air-filled region between the strips,

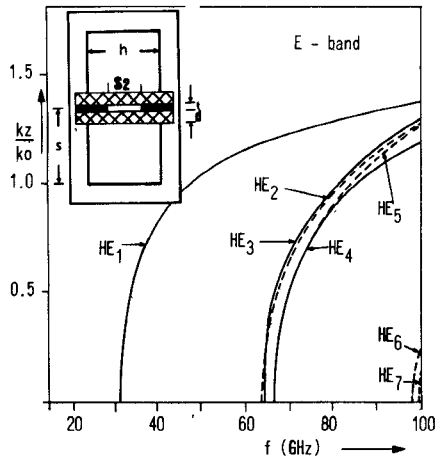

Fig. 10. Dispersion characteristic of a so-called insulated finline. $a = 3.1$ mm, $h = a/2$; $s = a/2$, $s2 = 0.6$ mm, $e = 0.5$ mm, $t = 5.$ μm, $d = 110.$ μm, $\epsilon_r = 3.75$. Symmetry plane at $s = a/2$: magnetic wall (——), electric wall (---------).

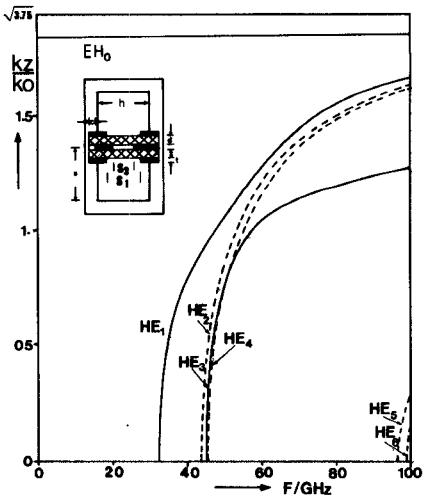

Fig. 13. Dispersion behavior of a single-side insulated finline combined with a bilateral finline. $s1 = 0.9$ mm, all other dimensions identical to Fig. 11.

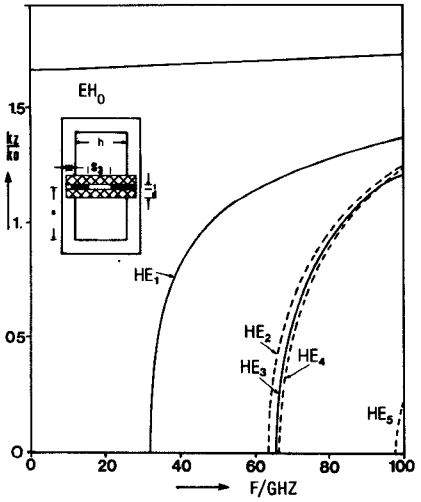

Fig. 11. Dispersion behavior of a single-side insulated finline. $a = 3.1$ mm, $h = a/2$; $s = a/2$, $e = 0.5$ mm, $c = s2 = 0.3$ mm (cf. Fig. 1(b)), $s3 = 0.6$ mm; $d = 110.$ μm, $\epsilon_r = 3.75$, $t = 5.$ μm. Symmetry plane at $s = a/2$: magnetic wall (——), electric wall (------).

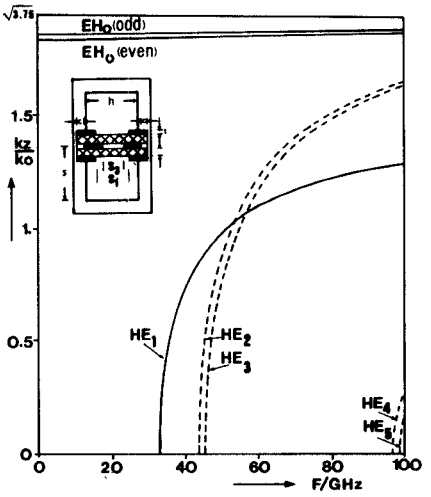

Fig. 14. Dispersion behavior of a dual-side insulated finline combined with a bilateral finline. Dimensions identical to Figs. 12 and 13.

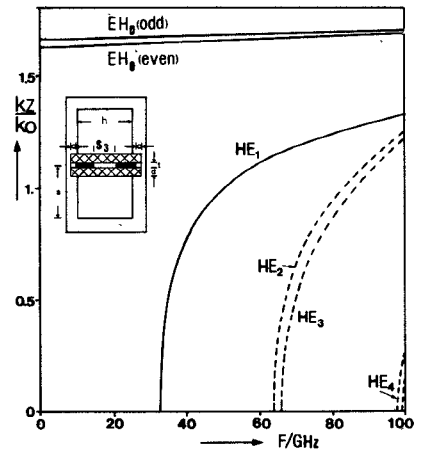

Fig. 12. Dispersion behavior of a dual-side insulated finline. $c = s2 = s4 = 0.3$ mm, all other dimensions identical to Fig. 11.

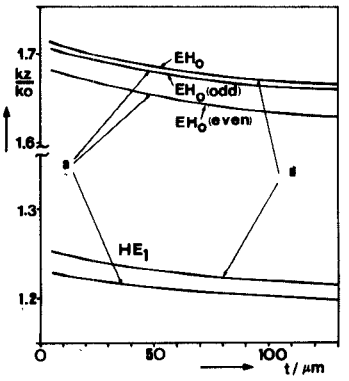

Fig. 15. Quasi-TEM and slot mode versus the metallization thickness, f-75 GHz. (a) Dual-side insulated finline (dimensions identical to Fig. 12. (b) Single-side insulated finline (dimensions identical to Fig. 11).

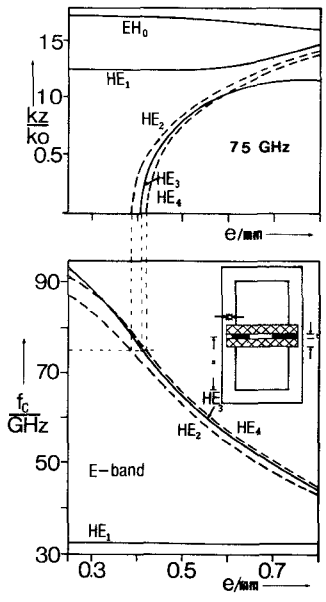

Fig. 16. Quasi-TEM and next higher order modes versus the groove depths e in a single-side insulated finline. f_c = cutoff frequency. Dimensions according to Fig. 11.

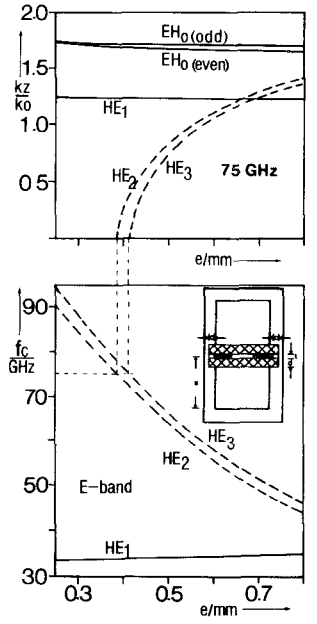

Fig. 17. Quasi-TEM and next higher order modes versus the groove depth e in a dual-side insulated finline. Dimensions according to Fig. 12.

resulting in a lower propagation constant when increasing the strip thickness.

Regarding the influence of the mounting grooves on the electrical characteristics of quasi-planar transmission lines, it was found out recently [6], [7] that higher order modes are strongly affected, whereas the HE_1 and the quasi-TEM modes are virtually insensitive to a wide range of changes in groove depth. In principle, this tendency is also observed for the single and dual insulated finline, and is shown in Figs. 16 and 17. For the single insulated configuration in Fig. 16, however, a mutual influence of the slot mode (HE_1) and the second higher order mode (HE_3) (which has the same field symmetry as the incident H_{10} mode) occurs, but was not observed for the dual-side insulated finline in Fig. 17. In that case (Fig. 17), both higher order modes (HE_2, HE_3) are obtained by considering an electric wall as the symmetry plane. It should be noted that, for operating frequencies beyond 75 GHz, the critical groove depth becomes shallower than given in Fig. 16, but can be increased a few percent by using a smaller substrate thickness.

IV. Conclusion

A versatile hybrid-mode analysis is presented taking into account the finite metallization thickness and mounting grooves in a class of various quasi-planar transmission lines. Using a modified mode-matching technique combined with a generalized transmission-line matrix exhibits the advantage of maintaining the size of the characteristic matrix equation constant even for an increasing number of discontinuities. Additionally, the method enables a user to create a modularized computer program which can easily be extended to a wide range of conceivable transmission-line configurations.

It is true that the method is not as fast as the spectral-domain technique; however, it includes the effect of finite metallization thickness and mounting grooves. Especially, the applications of quasi-planar transmission lines in the shorter millimeter-wave range have shown that the influence of the mounting grooves are more significant than the effect of finite metallization thickness. For example, a 0.7-mm-deep groove in a *Ka*-band waveguide mount causes a 2-GHz reduction of the cutoff frequency of the next higher order mode (Fig. 7), whereas the same groove depth reduces the next higher order mode in an *E*-band waveguide mount by at least 45 GHz (Fig. 16).

Appendix

Abbreviations for the partial wave amplitudes in (3) and (4) are

$$Im^{l}_{(n)}(x) = A^{l}_{(n)}e^{jkx^{l}_{(n)}x} + B^{l}_{(n)}e^{-jkx^{l}_{(n)}x}$$

$$Ue^{l}_{(n)}(x) = \frac{1}{jkx^{l}_{(n)}}\left\{C^{l}_{(n)}e^{jkx^{l}_{(n)}x} - D^{l}_{(n)}e^{-jkx^{l}_{(n)}x}\right\}$$

$$Ie^{l}_{(n)}(x) = C^{l}_{(n)}e^{jkx^{l}_{(n)}x} + D^{l}_{(n)}e^{-jkx^{l}_{(n)}x}$$

$$Um^{l}_{(n)}(x) = jkx^{l}_{(n)}\left\{A^{l}_{(n)}e^{jkx^{l}_{(n)}x} - B^{l}_{(n)}e^{-jkx^{l}_{(n)}x}\right\}.$$

The unknown coefficients $A^{l}_{(n)}$, $B^{l}_{(n)}$, $C^{l}_{(n)}$, and $D^{l}_{(n)}$ are eliminated by inserting the upper ($x = xo^{l}$) and the lower boundary ($x = xu^{l}$) values in the above equations. Thus, the generalized transmission-line matrix $\boldsymbol{R}^{l}$ for each subre-

gion contains the diagonal matrices

$$\boldsymbol{Rc}^{i} = \begin{bmatrix} \cos\left(kx^{i}_{(n)} xa^{i}\right) & \mathbf{0} \\ \mathbf{0} & \cos\left(kx^{i}_{(n)} xa^{i}\right) \end{bmatrix}$$

$$\boldsymbol{Rs}^{i} = \begin{bmatrix} -kx_{(n)} \sin\left(kx^{i}_{(n)} xa^{i}\right) & \mathbf{0} \\ \mathbf{0} & \dfrac{1}{kx^{i}_{(n)}} \sin\left(kx^{i}_{(n)} xa^{i}\right) \end{bmatrix}$$

$$\boldsymbol{Rs}^{i'} = \begin{bmatrix} \dfrac{1}{kx^{i}_{(n)}} \sin\left(kx^{i}_{(n)} xa^{i}\right) & \mathbf{0} \\ \mathbf{0} & -kx^{i}_{(n)} \sin\left(kx^{i}_{(n)} xa^{i}\right) \end{bmatrix} \quad xa = xo - xu$$

and the propagation constant

$$kx^{i}_{(n)} = \sqrt{ko^2 \epsilon^{i}_{r} - \left(ky^{i}_{(n)}\right)^2 - kz^2}$$

with $ko^2 = \omega^2 \mu_0 \epsilon_0$.

The functions $fc^{i}_{(n)}(y)$ and $fs^{i}_{(n)}(y)$ in (3) and (4) are determined by the boundary condition in the y-direction

$$fc^{i}_{(n)}(y) = \frac{\cos \widetilde{ky}^{i}_{(n)}}{\sqrt{1+\delta_{0n}}} \text{ and } fs^{i}_{(n)}(y) = \sin \widetilde{ky}^{i}_{(n)},$$

$$\delta_{0n} = \text{Kronecker delta.}$$

For example, $\widetilde{ky}^{4}_{(n)}$ in Fig. 2(a) means

$$\widetilde{Ky}^{4}_{(n)} = ky^{4}_{(n)} \cdot (y - b3), \qquad ky^{4}_{(n)} = \frac{n \cdot \pi}{b4 - b3}.$$

The coupling integrals $\boldsymbol{Fc}^{\nu}$ and $\boldsymbol{Fs}^{\nu}$ in (20) can be written as follows:

$$\boldsymbol{Fc}^{\nu}_{(nk)} = \int_{yu^{\nu}}^{yo^{\nu}} fc^{5}_{(n)}(y) fc^{\nu}_{(k)}(y)\, dy, \qquad \nu \in 4a, 4b, 4c$$

with $yu^{\nu} = (b7, b3, b5)$ and $yo^{\nu} = (b8, b4, b6)$.

For $\boldsymbol{Fs}^{\nu}$, replace fc with fs. The abbreviations for $\widetilde{\boldsymbol{Fc}}^{\nu}$ and $\widetilde{\boldsymbol{Fs}}^{\nu^T}$ in (20) and (21) are

$$\widetilde{\boldsymbol{Fc}}^{\nu} = \frac{2}{b2 - b1} \cdot \boldsymbol{Fc}^{\nu} \cdot \text{Diag}\left(ky^{\nu}_{(n)}\right)$$

$$\widetilde{\boldsymbol{Fs}}^{\nu^T} = \boldsymbol{Fs}^{\nu^T} \cdot \text{Diag}\left(ky^{\nu}_{(n)}\right).$$

$\boldsymbol{Fs}^{\nu^T}$ means the transposed of matrix $\boldsymbol{Fs}^{\nu}$.

ACKNOWLEDGMENT

The authors wish to thank Dr. W. J. R. Hoefer, University of Ottawa, and Dr. F. Arndt, University of Bremen, for helpful discussions and suggestions.

REFERENCES

[1] P. J. Meier, "Integrated fin-line millimeter components," *IEEE Trans. Microwave Theory Tech.*, vol. MTT-22, pp. 1209–1216, Dec. 1974.

[2] Y.-C. Shih and W. J. R. Hoefer, "Dominant and second-order mode cutoff frequencies in fin-lines calculated with a two-dimensional TLM program," *IEEE Trans. Microwave Theory Tech.*, vol. MTT-28, pp. 1443–1448, Dec. 1980.

[3] T. Itoh and A. S. Hebert, "A generalized spectral domain analysis for coupled suspended microstriplines with tuning septums," *IEEE Trans. Microwave Theory Tech.*, vol. MTT-26, pp. 820–826, Oct. 1978.

[4] L. P. Schmidt and T. Itoh, "Characteristics of unilateral fin-line structures with arbitrarily located slots," *IEEE Trans. Microwave Theory Tech.*, vol. MTT-29, pp. 352–355, Apr. 1981.

[5] L. P. Schmidt, "A comprehensive analysis of quasiplanar waveguides for millimeter-wave application," in *Proc. 11th Eur. Microwave Conf.* (Amsterdam), 1981, pp. 315–320.

[6] R. Vahldieck, "Accurate hybrid-mode analysis of various finline configurations including multilayered dielectrics, finite metallization thickness, and substrate holding grooves," *IEEE Trans. Microwave Theory Tech.*, vol. MTT-32, pp. 1454–1460, Nov. 1984.

[7] J. Bornemann, "Rigorous field theory analysis of quasiplanar waveguides," *Proc. Inst. Elec. Eng.*, vol. 132, pt. H, pp. 1–6, Feb. 1985.

[8] F. Arndt and G. U. Paul, "The reflection definition of the characteristic impedance of microstrips," *IEEE Microwave Theory Tech.*, vol. MTT-27, Aug. 1979.

[9] J. P. Villotte, M. Aubourg, and Y. Garault, "Modified suspended striplines for microwave integrated circuits," *Electron. Lett.*, vol. 14, no. 18, pp. 602–603, Aug. 31, 1978.

[10] W. Schuhmacher, "Wellentypen und Feldverteilung auf unsymmetrischen planaren Leitungen mit inhomogenem Dielektrikum," *Arch. Elec. Übertragung.*, vol. 34, pp. 445–453, 1980.

[11] J. Siegl, "Phasenkonstante und Wellenwiderstand einer Schlitzleitung mit rechteckigem Schirm und endlicher Metallisierungsdicke," *Frequenz*, vol. 31, pp. 216–220, July 1977.

[12] A. Beyer, "Analysis of the characteristics of an earthed fin-line," *IEEE Trans. Microwave Theory Tech.*, vol. MTT-29, pp. 676–680, July 1981.

[13] T. Kitazawa and R. Mittra, "Analysis of finline with finite metallization thickness," *IEEE Trans. Microwave Theory Tech.*, vol. MTT-32, pp. 1484–1487, Nov. 1984.

[14] H. Fritzsche, "Die frequenzabhaengigen Uebertragungseigenschaften gekoppelter Streifenleitungen im geschichteten Dielektrikum," *Nachrichtentech. Z.*, vol. 26, no. 1, pp. 1–8, 1973.

[15] R. Vahldieck and W. J. R. Hoefer, "The influence of metallization thickness and mounting grooves on the characteristics of finlines,"in *IEEE MTT-S Int. Microwave Symp. Dig.*, pp. 182-184.

Rüdiger Vahldieck (M'85) was born in Heiligenhafen, West Germany, in 1951. He received the Dipl.-Ing. and the Dr.-Ing. degrees, both in electrical engineering, from the University of Bremen, Bremen, West Germany, in 1980 and 1983, respectively. His Dr.-Ing. thesis was on the numerical analysis of generalized finline configurations and the de-

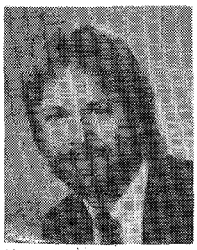

sign and development of low insertion loss finline filters.

From 1980–1983, he was a Research Assistant at the Microwave Department of the University of Bremen, where he was engaged in computer-aided design of millimeter-wave integrated circuits.

Since 1984, he has been a Post-Doctoral Fellow at the University of Ottawa, Ottawa, Canada. His research activities at present have chiefly been concerned with broad-band millimeter-wave couplers and different numerical techniques to solve electromagnetic field problems in finline structures.

Dr. Vahldieck is one of the recipients of the A. F. Bulgin Premium of the Institution of Electronic and Radio Engineers, 1983.

Jens Bornemann was born in Hamburg, West Germany, on May 26, 1952. He received the Dipl.-Ing. and the Dr.-Ing. degrees in electrical engineering from the University of Bremen, Bremen, West Germany, in 1980 and 1984, respectively.

Since 1980, he has been with the Microwave Department of the University of Bremen, where his current research activities include microwave integrated-circuit filter design, printed *E*-plane technology for millimeter-wave applications, and problems of electromagnetic-field theory, especially those requiring numerical methods of solution.

Dr. Bornemann is one of the recipients of the A. F. Bulgin Premium of the Institution of Electronic and Radio Engineers, 1983.